Journal of proteome research

pubs.acs.org/jpr

Article

A Sensitive and Controlled Data-Independent Acquisition Method for Proteomic Analysis of Cell Therapies

Camille Lombard-Banek,* Kerstin I. Pohl, Edward J. Kwee, John T. Elliott, and John E. Schiel*

Cite This: *J. Proteome Res.* 2022, 21, 1229−1239

Read Online

ACCESS | Metrics & More | Article Recommendations | Supporting Information

ABSTRACT: Mass spectrometry (MS)-based proteomic measurements are uniquely poised to impact the development of cell and gene therapies. With the adoption of rigorous instrumental performance qualifications (PQs), large-scale proteomics can move from a research to a manufacturing control tool. Especially suited, data-independent acquisition (DIA) approaches have distinctive qualities to extend multiattribute method (MAM) principles to characterize the proteome of cell therapies. Here, we describe the development of a DIA method for the sensitive identification and quantification of proteins on a Q-TOF instrument. Using the improved acquisition parameters, we defined a control strategy and highlighted some metrics to improve the reproducibility of SWATH acquisition-based proteomic measurements. Finally, we applied the method to analyze the proteome of Jurkat cells that here serves as a model for human T-cells. Raw and processed data were deposited in PRIDE (PXD029780).

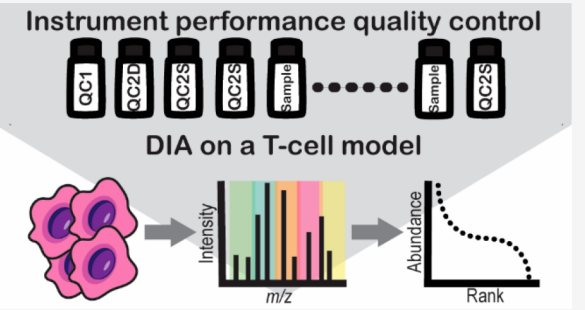

KEYWORDS: *data-independent acquisition, SWATH acquisition, cell therapies, biopharmaceutical, mass spectrometry, bottom-up proteomics, performance qualification (PQ), quality control (QC)*

INTRODUCTION

Complex therapies, whereby viruses or whole cells act as the drug, are emergent new treatments requiring new characterization strategies. For example, chimeric antigen receptor T-cells (CAR-Ts) are modified patient T-cells that utilize the existing biological properties of these immune cells to target and kill cancer cells. CAR-Ts are obtained by engineering the patient's T-cells to express a receptor on their surface—the CAR—specific to the surface receptors on the targeted malignancy. The genomic information for the CAR protein is incorporated in the cell via transduction with a viral vector (retrovirus or lentivirus).[1] A series of complex cell sorting, activation, and expansion steps are required before reintroducing the transduced CAR-T cell product back into the patient. Details on the manufacturing of CAR-T cells are available in recent reviews.[1,2]

Current state-of-the-art analyses of CAR-T drug products rely on the measurements of a few select proteins.[3−5] For example, fluorescence-activated-cell sorting (FACS) measures T-cell population purity and CAR expression using fluorescently labeled antibodies against T-cell surface markers (CD4 and/or CD8) or the CAR, respectively. The drug's pharmacological activity is assessed via activation using beads decorated with the tumor surface receptor followed by cytokine-release assays.[3,4,6] Cytokine-release assays measure signaling proteins (interleukin, interferon, and growth factors) released by the CAR-Ts. Although useful, these assays only measure a limited number of quality attributes of the raw material (T-cells) or the product (CAR-Ts). Identifying attributes that better predict the quality of the product could better position these drugs from a last resort to the second or first line of treatments, which requires better characterization of the manufacturing process and the final product.[4,7]

MS enables the characterization of a large number of proteins in a single label-free (i.e., no antibodies) experiment.[8,9] We have recently reviewed the potential benefits of MS-based proteomics in addressing the challenges to characterize cell therapies.[8] Two main data acquisition strategies exist to measure proteins in an untargeted fashion (also referred to as shotgun approaches): data-dependent and data-independent acquisitions (DDA and DIA, respectively). In DDA, peptide ions are selected for fragmentation using a narrow isolation window following a top-N scheme.[10,11] In a top-N scheme, the N most abundant precursor ions are selected for fragmentation per instrument cycle time. The fundamental nature of DDA renders the identification of the same peptide/proteins in replicate runs stochastic. Therefore,

Received: November 18, 2021
Published: April 11, 2022

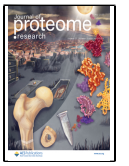

label-free quantification using DDA often leads to missing peptide information across replicates, referred to as missing values, which decreases quantitative coverage and statistical power. Strategies such as multiplexing with isobaric tags partially remediate the issue, albeit at a high cost.[11,12] Conversely, in DIA, broad isolation windows scanning across the entire m/z range enable the fragmentation of all peptide ions regardless of their intensity, leading to a significant decrease in missing values.[3,13,14] Mirroring the current multi-attribute-method (MAM) employed for single protein-drug molecules,[15−17] DIA can quantify multiple proteins with high precision for more complex biopharmaceutical systems like cell therapies. In MAM, a preliminary run is performed in DDA mode to determine the list of peptide identities and their respective retention times. Consecutive runs are then performed and compared in MS-only mode (no fragmentation) to quantify peptides of interest.[15] Similarly, in DIA, DDA is performed first to build a list of peptide-query-parameters (PQPs) used to extract peptide and protein identities from raw DIA. PQPs encompass fragment ion (transition) lists for each identified peptide and their respective retention times.[18] Proteins are quantified using the sum of the integrated area under the extracted chromatogram curve of the peptide fragment ions.

During MS-based proteomic analysis, multiple factors that have been summarized elsewhere[19−21] contribute to the technical variability of the measurements. NanoLC-MS instruments contribute in large part to the measurement variability. The National Institute of Standards and Technology (NIST) and the National Cancer Institute (NCI) have established 46 metrics to evaluate the performance of LC-MS systems, called Mass Spectrometry Quality Control (MSQC). These 46 metrics correspond to 6 categories critical to LC-MS measurements: chromatography, dynamic sampling, ion source, MS1 signal, MS2 signal, and peptide identification.[20] Several informatics tools have been developed to monitor instrument performances.[21−24] Now, technical variability in large-scale bottom-up proteomics by DIA can be assessed using these principles and experimental design borrowed from MAM and/or clinical proteomics.[8]

MS-based proteomics has proven beneficial to shed light on the mechanism of action of CAR-Ts[25−27] and is poised to identify additional process and/or product quality attributes by monitoring cell health at critical stages of the manufacturing process. Expansion of large-scale MS-based proteomics from the research setting to the process development requires stringent performance qualifications (PQs) to be fit-for-purpose. Here, we describe the development of a sensitive and controlled MS-based proteomic acquisition method on a quadrupole time-of-flight system using DIA toward the analysis of CAR-T cell therapies. We first established the different conditions that provided the highest sensitivity and reproducibility, including the separation, data-dependent acquisition for PQPs library building, and DIA for quantification. Then, we provide guidelines and metrics to extend DIA from a research setting to the biopharma space using the MSQC principles. Finally, we applied the strategy to the measurement of a Jurkat cells digest. Jurkat cells are immortalized lymphoblastic T-cells and are being used to produce CAR-T mimetic to be employed as a method development tool and system suitability test.[28]

EXPERIMENTAL SECTION

Reagents

Reagents were purchased at reagent grade or higher. Standard K562 protein digests were from SCIEX (Framingham, MA) or Promega (Madison, WI). PepCalMix, containing 20 heavy labeled peptides were from SCIEX. Dithiothreitol (DTT, #39255) and iodoacetamide (IAA, #39271) were procured in no-weigh format from Thermo Fisher Scientific (Waltham, MA). MS-grade trypsin/Lys-C protease mix was from Thermo Fisher Scientific (#A41007). Solvents for liquid-chromatography (LC) mass spectrometry (MS) measurements were purchased at LC-MS grade from Honeywell (Charlotte, NC).

Preparation of Peptide and Protein Digest Standards

Commercial PepCalMix (SCIEX), containing 20 heavy labeled peptides, at a concentration of 1 pmol/μL (stock solution). Aliquots of 10 μL each were stored at −80 °C until further use. For nanoLC-MS measurements, 1 μL of the PepCalMix aliquot was diluted in 99 μL of 5% v/v acetic acid in 10% v/v acetonitrile containing water (final peptide concentration: 10 fmol/μL).

Commercial K562 digests were reconstituted to 2 μg/μL in 0.1% v/v formic acid in water and stored at −80 °C in 10 μL aliquots. Prior to nanoLC-MS measurements, 9 μL of 0.1% v/v formic acid in 2% v/v acetonitrile containing water and 1 μL of the stock PepCalMix solution (1 pmol/μL) were added to the 10 μL K562 digest aliquot. The final K562 peptide concentration was 1 μg/μL.

To assess the sensitivity of our acquisition method, we built the calibration curve using the PepCalMix. Different amounts of PepCalMix were spiked into a 0.5 μg/μL K562 digest solution. A total of 6 dilutions were prepared with the following final PepCalMix concentrations: 0.01, 0.1, 1, 10, 50, and 100 nmol/L.

Jurkat Cell Culture and Preparation for Proteomic Analysis

Jurkat cells (ATCC) were cultured in T-75 flasks using RPMI-1640 media (ATCC) supplemented with 10% heat-inactivated fetal bovine serum (Gibco). Cells were passaged to maintain a cell density between 2×10^5 to 2×10^6 cells/mL. The desired number of cells was counted using a Multisizer 3 Coulter Counter (Beckman Coulter, Sykesville, MD) and aliquoted into Protein LoBind Tubes (Eppendorf). Cells were washed three times with Dulbecco's phosphate buffered saline without calcium and magnesium (Gibco), centrifuging at 200g between washes. Cells were frozen at −20 °C.

Jurkat cells digests were obtained following the manufacturer-recommended S-TRAP (Protifi, Farmingdale, NY) protocol. Briefly, 5×10^6 cells were lysed with 50 μL of lysis solution provided in the S-TRAP mini kit. Cysteine residues were reduced (50 mmol/L DTT, 20 min, 75 °C, 1000 rpm) and alkylated (150 mmol/L IAA, 20 min, RT. The protein extract was acidified with 5 μL of 12% v/v phosphoric acid. Then, 350 μL of 90% v/v methanol in 100 mmol/L triethylamine bicarbonate (TEAB) were added to the protein solution, which was then loaded onto the S-TRAP column. Proteins were digested with 7.5 μg of trypsin/Lys-C in 100 mmol/L TEAB for 1.5 h at 47 °C. Peptides were recovered by centrifugation at 1000g for 1 min and successive addition of 0.2% v/v formic acid in water and 0.2% v/v formic acid in 80% v/v acetonitrile in water. Finally, the sample was dried to completeness in a vacuum concentrator (Labconco; Kansas City, MO)

https://doi.org/10.1021/acs.jproteome.1c00887
J. Proteome Res. 2022, 21, 1229−1239

Peptide Separation by NanoLC

Peptide separation was performed using an Eksigent NanoLC 425 system (SCIEX, Framingham, MA) in a nanoflow setting with trap and elute configuration. Peptide samples were loaded onto a C18 trap column (ChromXP C18−3 μm and 120 Å, Eksigent, 350 μm × 0.5 mm, Part #5016752) using an isocratic delivery of 100% solvent A (water containing 0.1% v/v formic acid) at a flow rate of 2 μL/min for 5 min. Then, peptides were separated on a nanoLC column. The organic solution (solvent B) was composed of acetonitrile with 0.1% v/v formic acid. The different columns tested, their properties, and the gradient conditions used for the K562 samples are recapitulated in Table S1. Once the ideal column condition was established for our experiment, peptides were separated on a nanoAcquity nanoLC column (Waters, Wilford, MA, 75 μm × 250 mm) packed with BEH-C18 (1.7 μm × 300 Å) at a flow rate of 200 nL/min. PepCalMix samples were separated using the following 13 min gradient starting at 2% solvent B: 12 min 40% solvent B; 13 min 80% solvent B; 17 min 2% solvent B. The different elution gradients for the K562 digest sample are reported in Table S2. Peptide samples prepared to test the instrument/method sensitivity and the Jurkat digest samples were separated using the 90 min gradient listed in Table S2.

Data-Dependent Acquisition Mass Spectrometry

Eluting peptides were ionized using an OptiFlow Turbo V ion source (nanoESI) and mass analyzed and detected in the positive ion mode by a fast-scanning quadrupole-time-of-flight instrument (TripleTOF 6600+ system, SCIEX, Framingham, MA). The initial acquisition method was set as a "top 30" experiment. TOF-MS scans were acquired with an accumulation time of 250 ms over the m/z range 400 to 1250. Precursor ions were selected for fragmentation with 0.7 amu isolation width, fragmented by CID with nitrogen using manufacturer optimized rolling collision energy. MS/MS spectra were collected in high-sensitivity mode for ions presenting charges between 2 and 5, counts per second above 150, with the following settings: accumulation time, 50 ms and m/z range, 100 to 1500, dynamic exclusion on for 7 s for columns #1 and #2 and for 5 s for column #3, #4, and #5. Any changes applied for DDA method development purposes are summarized in Table S3.

Data Independent Acquisition (SWATH Acquisition)

The same ionization conditions and instruments were used for the DDA methods. Initially, TOF-MS scans were acquired with the following parameters: accumulation time, 50 ms; m/z range, 400 to 1250. Consecutive SWATH acquisition scans were acquired with the following conditions: accumulation time, 50 ms; m/z range, 100 to 1500; SWATH acquisition window, 20 amu with 1 amu overlap. For method evaluation purposes, the isolation window schemes and the mass ranges were changed and are reported in Table S4 and Table S6.

Database Search and Protein Identifications

Raw mass spectra acquired by DDA were processed for protein identification in ProteinPilot software running the Paragon search engine[29,30] (v5.0.2.0, SCIEX). MS/MS spectra were searched against the SwissProt canonical human database (containing 20,396 entries). The search was performed in "Thorough ID" mode, which automatically adjusts the mass tolerance to the resolution of the MS and MS/MS acquisitions. Carbamidomethylation of cysteines, trypsin for digestion, and TripleTOF 6600+ system were set as search defaults. "Thorough ID" mode allows all possible variable modifications including up to 2 missed cleavages per peptide. Protein and peptides are reported with 1% false discovery rate (FDR). Proteins are reported with a minimum of 1 peptide identification above 95% confidence. The lists of proteins identified by DDA for each condition are available in Table S5.

Protein Quantification

Peak extractions from the DIA experiments were performed in PeakView software 2.0 using the SWATH acquisition microapp (SCIEX) using DDA-generated PQPs libraries. The PQPs were generated for nonredundant and unmodified peptides identified from a combined search of K562 and Jurkat samples (total of 26 DDA MS files) in ProteinPilot software. The following criteria were used for MS/MS peak extraction and protein quantification: 6 transitions/peptide; 10 min retention time tolerance; 75 ppm mass tolerance; peptide identification scoring less than 1% FDR; up to 6 peptides/protein. Retention times were aligned using the spiked in PepCal Mix. The peakView software only allows for setting 1 transition per peptide and 1 peptide per protein. Extracted peptides were filtered for 1% FDR. Quantified proteins were filtered to contain a quantitative value across all three replicates. The lists of proteins quantified by SWATH acquisition are available in Table S6.

Statistical Data Analysis

Data analysis and parsing were performed using custom scripts in R language running in Rstudio. All measurements were performed in technical triplicates to calculate the means and the relative-standard-deviations (RSDs).

Data and Script Sharing

Scripts used for the analyses of data are made available on GitHub (https://github.com/Lombardbanekc/CART-SWATH-MS-Data-Processing.git). RAW data and search results files for DDA and DIA experiments have been deposited to the ProteomeXchange server (PXD029780).

RESULTS AND DISCUSSION

Designing a Sensitive, Reproducible, and Controlled Method to Quantify Proteins from Cells

Multiple components of the data acquisition workflow were evaluated to enable a sensitive and robust quantification of the proteome of cell-based therapies and to provide suggestions for best practices on implementing instrument controls to expand the application of DIA to the biopharma space. Figure 1 summarizes our approach. First, we revised the chromatography by evaluating a total of five reversed-phase (C18) commercial columns from three different vendors (see Table 1), and we then evaluated different tuning parameters for DDA and DIA (Table S3 and Table S4). Although our main application is to perform DIA for quantification, DDA evaluation is still critical as it is used to build the list of PQPs necessary to extract peptide signals and identify proteins from DIA raw files.[18]

The chromatography is a critical component of nanoLC-MS-based proteomic experiments because improved separation can notably enhance method sensitivity.[31−33] For example, reducing the column diameter and support particle size improved peak shape and increased the signal-to-noise ratio for peptides by ≈2-fold.[34] Tuning the MS parameters to fit the application has also been shown to be sometimes valuable in increasing the proteome coverage. Multiple studies using TOF

https://doi.org/10.1021/acs.jproteome.1c00887
J. Proteome Res. 2022, 21, 1229−1239

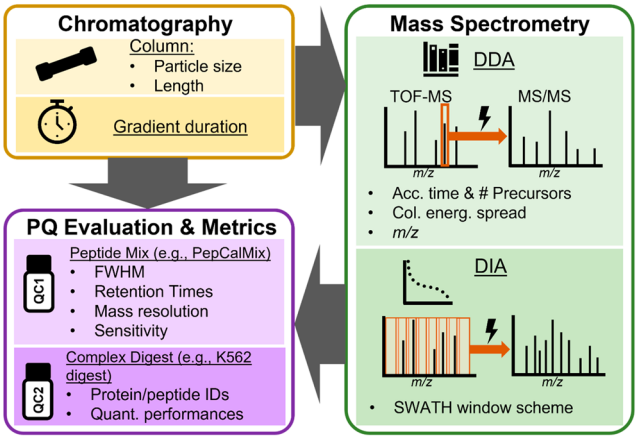

Figure 1. Overview of the analytical measurement parameters that were evaluated to build a sensitive method and draw our instrument performance qualifications (PQ) metrics.

or trapping instruments such as Orbitraps have evaluated the importance of some acquisition parameters in improving the number of proteins identified/quantified.[35−38] For DDA experiments, the chromatographic conditions and the acquisition parameters were evaluated based on the numbers of peptides and proteins identified with 1% FDR. For DIA experiments, we evaluated the numbers of peptides and proteins quantified, the quantification range, and the reproducibility of the quantification measured by the RSD. Once our method was established, we devised an instrument control strategy and defined some metrics to survey to strengthen the applicability of our developed method to biopharmaceutical products like cell therapies (Figure 1). Finally, we applied our method to Jurkat cells, an immortalized cancer T-cell cell line currently used to build precompetitive CAR engineered cells.[28]

Evaluating the Importance of the Chromatography in Improving the Identified Proteome Coverage

We evaluated the peptide separation for both DDA and DIA in tandem to make a concerted decision on the column to choose for our application. Each column tested was selected to represent different particle sizes, pore sizes, lengths, and support particle properties. The properties of each column are recorded in Table 1, and the gradients used for each column are summarized in Table S1. In this study, we purposely kept the vendors and models hidden to remain partial, as commended by the NIST mission. The goals of the evaluation are (1) to demonstrate that different performance metrics are unique to the instrument setup and (2) to evaluate the effect of the column properties on the measurements. During DDA, using 1 μg of a commercial K562 digest on the column, we found that the columns with the smallest particle size led to much higher numbers of peptides and proteins identified per run; more than 3000 proteins were identified per replicate for each of these 3 columns (Table 1). The proteins identified using the different columns were mostly complementary (Figure 2A). Columns #4 and #5, which were the longest, demonstrated many unique proteins identified compared to the other three (Figure 2A). The increase in proteins identified using the columns with the smallest particle size (columns #3, #4, and #5) was proportionally distributed across the three main cell compartments: Cytosol, nucleus, and membrane (Figure 2B). This finding suggests that none of the columns were biased toward the cellular location of the proteins.

Next, we evaluated each column for DIA, using 500 ng (Figure 2CD) and 200 ng (Figure S1) of K562 protein digest on the column. For consistency, we processed the DIA data from each column using the same list of PQPs obtained as described in the Experimental Section. Retention times were aligned using the spiked in PepCalMix (20 heavy labeled peptides), and the same parameters were used to extract the data (see Experimental Section). Figure 2C shows the number of proteins quantified as well as their dynamic range. All five columns presented a similar dynamic range of ≈5 orders of magnitude. Surprisingly, column #3 underperformed—fewer proteins were quantified than with the other four columns, despite having good results in DDA experiments. Column #5 performed the best with close to 3000 proteins quantified across all three replicates using 500 ng of protein digest, which is ≈13% more than the next best one—column #4 (Figure 2C). Moreover, when analyzing only 200 ng of digest, we still quantified ≈2650 proteins using column #5 (Figure S1A). We evaluated the repeatability of our quantification by measuring the RSD across technical triplicate measurements (Figure 2D and Figure S1B). For all the columns, the median RSDs were below 15%, demonstrating the quality of DIA quantification measurements. Interestingly, the distribution of RSDs for the shorter columns (columns #1, #2, and #3) spread more than for the two longer columns (columns #4 and #5). Column #5 presented an outstandingly low median RSD of ≈4% (Figure 2D) and a tight distribution around the median value. The RSD values were only slightly increased when measuring 200 ng (Figure S1B).

On the basis of the different properties of the chosen columns, we can attribute the improvement in the numbers of proteins identified and quantified using columns #4 and #5 to two main factors: Particle size and column length. These results are not particularly surprising and have been well documented previously for DDA-only experiments.[31,34] Here, we demonstrated that these important column attributes also

Table 1. Summary of the Properties of the Five Columns Tested and the Corresponding Number of Identifications by DDA from 1 μg Injections of K562 Commercial Digest[a]

column #	vendor	length (cm)	particle size (μm)	pore size (A)	# peptide identified	# protein identified
1	A	15	3	120	17614 ± 186 (22717)	2599 ± 34 (2969)
2	B	15	3	300	18071 ± 590 (22473)	2613 ± 78 (2961)
3	C	15	1.7	130	23081 ± 468 (28231)	3228.3 ± 14 (3550)
4	C	25	1.7	130	28794 ± 131 (35336)	3557 ± 21 (3968)
5	C	25	1.7	300	29772 ± 184 (36151)	3774 ± 165 (4120)

[a]Error is represented by the standard deviation of the number of identifications. Numbers in parentheses represent the combined identifications from triplicate measurements.

https://doi.org/10.1021/acs.jproteome.1c00887
J. Proteome Res. 2022, 21, 1229−1239

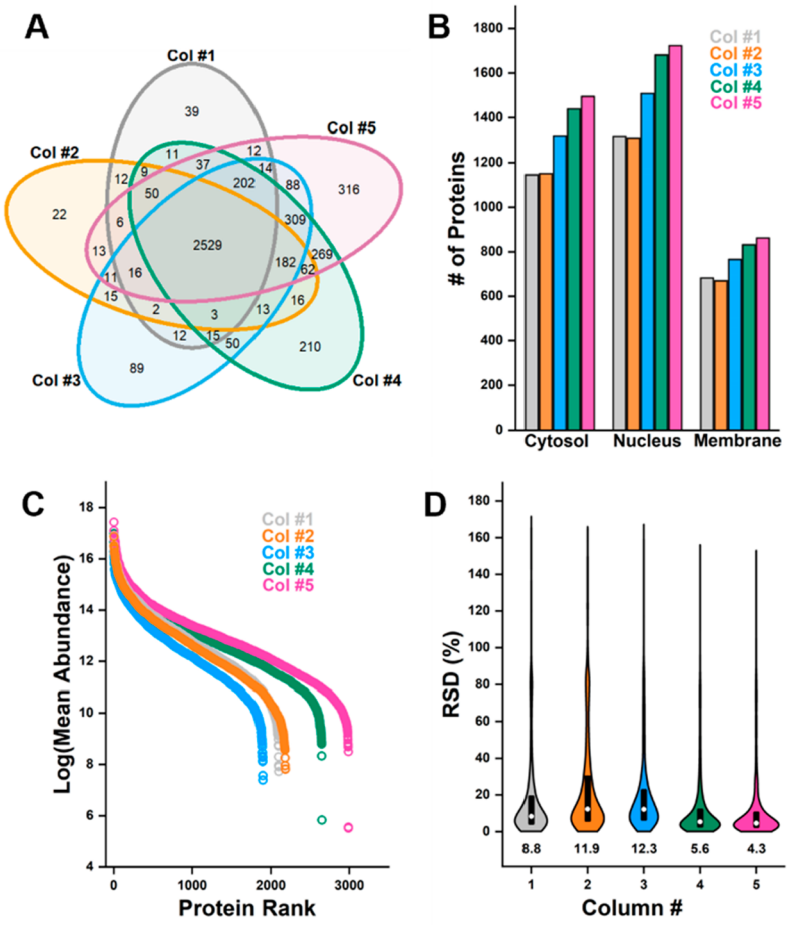

Figure 2. Column evaluation on protein identification and quantification using the 90 min gradients described in Table S1. (A) Venn diagrams showing the overlap of proteins identified from combined replicate DDA runs between all five columns from 1 μg of K562 digest. (B) Distribution of the identified combined proteins' cell compartment for each column conditions. (C) Quantitative dynamic range for each column by DIA for 500 ng of K562 digest. (D) Quantitative reproducibility of the quantification between technical replicates as measured by the RSD.

play a critical role in the quality of the DIA-based quantification, as illustrated by the low median RSDs obtained when using columns #4 and #5. These improvements can be attributed to better chromatographic properties. Indeed, increased resolution of the chromatographic separation and improved chromatographic peak shapes lead to better peak extraction of DIA data. Better resolution of the chromatographic separation decreases the occurrence of coeluting peptides, which decreases tandem mass spectra complexity; better peak shape improves peak statistics. Overall, DDA and DIA-based quantitative results suggested that column #5 was the most favorable for our future experiments and was used for the remainder of this study.

The gradient duration on column #5 was further refined using 500 ng of K562 digest (Figure 3A,B). We aimed to balance gain in protein identifications and throughput and evaluated 4 different gradient durations for DDA experiments: 45, 60, 90, and 120 min. Peptide elution windows of 90 and 120 min are standard for untargeted large-scale bottom-up proteomic experiments by DDA. We also considered shorter gradients, not typically used in large-scale bottom-up proteomics, due to the fast-scanning rate of our quadrupole-time-of-flight instrument. As DDA experiments are here used to build PQP libraries, we purposely report the combined number of protein identifications (Figure 3A and Table S5). Interestingly, we found that the gain in the number of protein identifications got smaller as we increased the gradient duration (Figure 3A). When increasing from 90 to 120 min, the number of identified proteins improved by ≈6%, while the throughput decreased by ≈30% (Figure 3A). The mitigated improvement as the gradient time increased can be attributed to the increase in chromatographic peak width and acquisition redundancy (Figure S2).

DIA runs are typically acquired using similar or shorter gradient than for DDA. Therefore, as we established a 90 min gradient for DDA runs, we eliminated the 120 min gradient from the evaluation for DIA. In DIA, the increases in protein identifications were lesser than with DDA (Figure 3B). Indeed, we only notice an increase of a maximum of 5% when lengthening the gradient duration using the traditional DIA method. It is worth noting that, unlike with DDA, the % increase was more prominent as we lengthened the gradient duration. However, this observation could reflect a bias in data analysis since the PQP library was built using a 90 min gradient.

Changing the gradient also impacted the reproducibility of the quantification. With 90 min gradient, the percent of proteins quantified with a percent relative standard deviation (% RSD) below 10% is higher than with 60 or 45 min gradients (≈55% vs ≈46% and 43%, Figure S2A); the percent

https://doi.org/10.1021/acs.jproteome.1c00887
J. Proteome Res. 2022, 21, 1229−1239

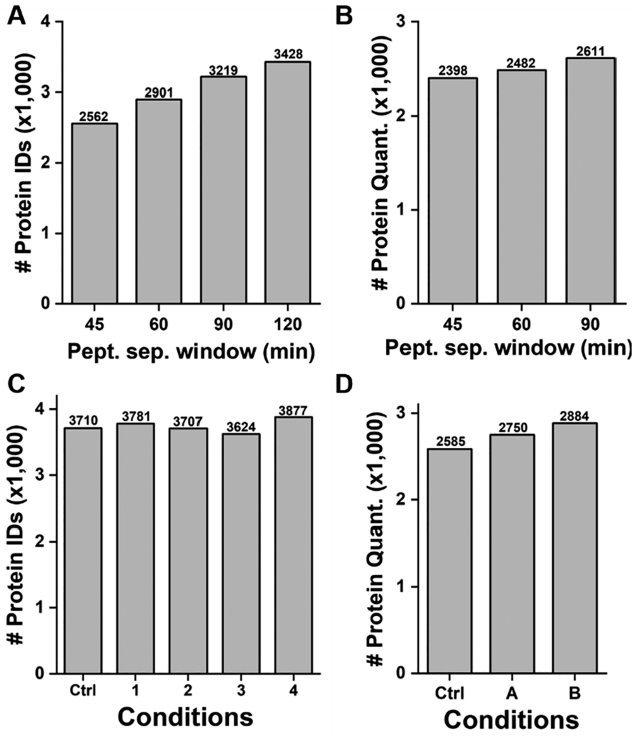

Figure 3. Revision of the acquisition conditions for DDA and DIA modes using 500 ng on-column of a K562 digest. DDA results are shown for combined data from three technical replicates. Protein identifications from DIA were filtered to include proteins that had quantification values across all three replicates. (A,B) The gradient length was evaluated for DDA (A) and DIA (B) modes. Gradient descriptions are available in Table S2. (C) Several acquisition parameters were studied for DDA acquisition. Details are reported in Table S3. (D) The window scheme was evaluated for DIA. Conditions are described in Table S4. Key: # Protein IDs, Numbers of protein identified; # Protein Quant., Numbers of protein quantified; Pept. sep. window, Peptide separation window; ctrl, control.

of protein quantified with % RSD below 20% is the highest with 60 min gradient (≈79% vs ≈73%, Figure S2A). Overall, we noted that the gradient length played a minor role in improving the number of proteins identified and quantified in DIA, especially compared to the notable improvements resulting from the column change. Most recently, using the newest generation LC system, quantification of ≈2000 proteins was achieved in a 1 min span using this type of instrument and an advanced DIA strategy.[39]

Evaluation of the MS Acquisition Parameters on the Protein Identification and Quantification

Using column #5 and a 90 min gradient, we assessed the role of parameters, deemed critical by the instrument vendor, in improving the number of proteins identified by DDA and the quality of protein quantified by DIA (Figure 3CD). For DDA, we evaluated the number of precursors selected per instrument cycle, the TOF-MS accumulation time, and the collision energy spread (CES). The number of selected precursors and the TOF-MS accumulation time were adjusted in unison to maintain the cycle time constant. MS acquisition parameters are recapitulated in Table S3. Each change was evaluated against the suggested method from the SCIEX performance evaluation guidebook (ctrl, Figure 3C). We tested adjusting the cycle time to 1.2 s to match the median chromatographic peak width (fwhm) of 12s, resulting in fewer proteins identified (data not shown). Lowering the TOF-MS accumulation time and increasing the number of selected precursors (cond1) improved the identification numbers the most (≈2%, Figure 3C). We also evaluated the effect of adding CES to fragment peptides. When using a CES, peptides are fragmented in 10 increments of collision energy (CE), spanning CE−CES to CE+CES, over the TOF-MS/MS accumulation time (here 50 ms). We found that setting the CES to 3 (cond2, Figure 3C) gave better results. Finally, for our final method, we combined the values that led to the highest improvements in identification and adjusted the m/z TOF-MS scan range to more closely match the span of m/z values present in the digest (Figure S4). We found that changing the m/z range did not affect the number of protein and peptide identifications (data not shown). However, the m/z range affects the DIA by reducing the number of fragmentation windows, leading to a lower cycle time for the same window width and providing better chromatographic peak statistics for reproducible quantification. Pino et al. recently demonstrated the advantages of a narrower m/z scan range for DIA on trapping instruments.[38] The cumulative advantages of more precursors selected and improved CES led to an ≈5% increase in protein identified. This improvement, although small, led to an expansion of the list of PQPs for SWATH acquisition data processing.

For DIA, we only evaluated the windowing scheme. All DIA data were searched against the same list of PQPs as defined in the method section. The different conditions were evaluated against the suggested method provided by SCIEX, which uses a 32 fixed windows scheme, but with the TOF-MS m/z scan range adjusted to our sample of choice: 375 to 1000 (ctrl, Figure 3D). Condition A (condA) and B (condB) were based on a 32 and 30 variable windows scheme, respectively. We found that 30 variable windows led to higher numbers of protein quantified with an ≈12% increase compared to the control. Interestingly, the number of proteins with % RSD lower than 10% was the same across all three conditions (Figure S3B), but the number of proteins with % RSD below 20% was lower with the variable window schemes (69% vs 65%, Figure S3B). It is likely due to the variable window scheme methods identifying more lowly abundant proteins compared to the fixed window scheme (Figure S5).

Evaluation of DIA Method Sensitivity

From the above method revisions, we determined the following DIA parameters: Separation, Column #5 and 90 min gradient; DIA, condition B. Using this method, we evaluated the quantitative performances of our approach by DIA. We established the sensitivity of our DIA method by creating samples containing different concentrations of the PepCalMix (0.01−100 nmol/L) in a constant K562 cell digest background. This sample mix better represents complex peptide samples, which can suffer major interferences due to coeluting and cofragmenting peptides during SWATH acquisition analyses. After extracting the data using the PeakView software, we built calibration curves to establish our analytical method's lower limit of detection (LLOD) and lower limit of quantification (LLOQ). A representative calibration curve for peptide sequence AVGANPEQLTR (m/z 583.3136, z = 2+) is presented in Figure S6. Results for all peptides are presented in Table 2. Out of 19 peptides detectable in the method m/z range, we confidently detected

https://doi.org/10.1021/acs.jproteome.1c00887
J. Proteome Res. 2022, 21, 1229−1239

Table 2. Quantification Sensitivity Measured Using Spiked in PepCalMix into a K562 Digest with a 90 min Gradient (Table S1) on Column #5 and the DIA Condition B (Table S4)[a]

sequence	m/z	z	LLOQ (nmol/L)	LLOD (nmol/L)	R^2
AETSELHTSLK	408.5501	3	1	<0.01	0.89
GAYVEVTAK	473.2602	2	0.1	0.01−0.1	0.95
IGNEQGVSR	485.2530	2	ND	ND	NA
LVGTPAEER	491.2656	2	1	<0.01	0.94
LDSTSIPVAK	519.7997	2	0.1	0.01−0.1	0.93
AGLIVAEGVTK	533.3233	2	0.1	<0.01	0.95
LGLDFDSFR	540.2734	2	1	<0.01	0.84
GFTAYYIPR	549.2863	2	0.1	<0.01	0.95
SGGLLWQLVR	569.8340	2	ND	ND	NA
AVGANPEQLTR	583.3136	2	0.1	<0.01	0.99
SAEGLDASASLR	593.8005	2	0.1	<0.01	0.95
VFTPLEVDVAK	613.3496	2	0.1	<0.01	0.90
VGNEIQYVALR	636.3527	2	0.1	<0.01	0.95
YIELAPGVDNSK	657.3450	2	0.1	0.01−0.1	0.91
DGTFAVDGPGVIAK	677.8583	2	ND	ND	NA
YDSINNTEVSGIR	739.3615	2	1	<0.01	0.96
SPYVITGPGVVEYK	758.9105	2	0.1	<0.01	0.96
ALENDIGVPSDATVK	768.9034	2	0.1	<0.01	0.96
AVYFYAPQIPLYANK	883.4738	2	0.1	<0.01	0.99

[a]A representative example of the calibration curves is presented in Figure S6. Key: LLOQ, lower limit of quantification; LLOD, lower limit of detection; ND, non detected.

16 of them. The three peptides labeled as nondetected did not pass the FDR cutoff of 1%, likely due to the presence of interfering peptides from the K562 digest (Table 2). The majority of the 15 peptides had an LLOQ of 0.1 nmol/L, and four peptides had an LLOQ of 1 nmol/L. Considering that 1 μL of the sample mixture was injected into the column for analysis, the absolute LLOQs are 0.1 fmol and 1 fmol, respectively. For most peptides, we never reached the LLOD, and so we noted the LLOD to be below our last measured concentration of 0.01 nmol/L (10 amol). For three peptides, the LLOD was estimated to be between the last two measured concentrations, 0.01 and 0.1 nmol/L or 10 to 100 amol (Table 2).

These LLOQs and LLODs values demonstrate very good sensitivity over a broad range of peptide properties. It raises confidence in the ability of the method to quantify proteins present in cells at low levels in an untargeted manner.

Establishing a Performance Qualification (PQ) Strategy for DIA

We designed a PQ strategy to ensure reproducible analysis of scarce material such as engineered T-cells. The design of our control strategy responds to the MSQC principles as described in the introduction.[20] Figure 4 highlights the overall strategic design and some figures of merit for controlled parameters. Two primary samples are used for PQ. In our case, one is a simple mixture of peptides (QC1)—PepCalMix (20 heavy labeled peptides, ABSCIEX); the other is a complex commercial K562 cell digest (QC2, Figure 4A). The PepCalMix is used to control the chromatographic separation, ionization efficiency, MS1 signal, MS2 signal, and perform

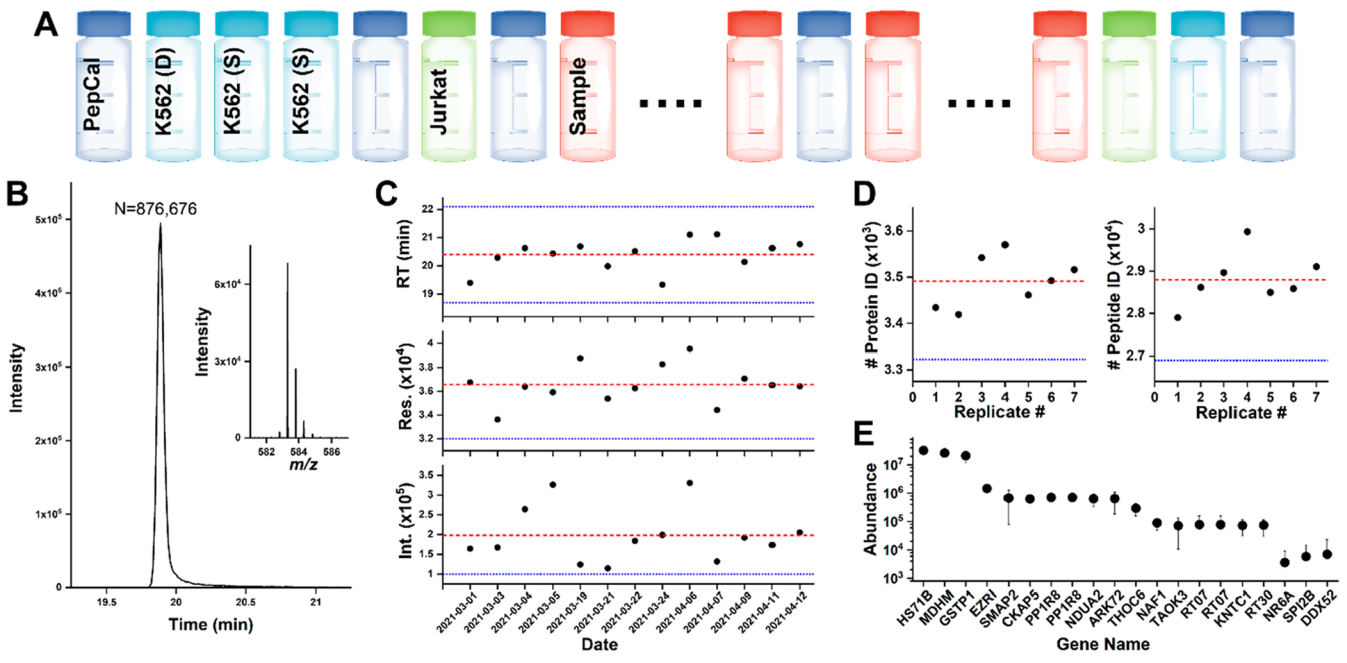

Figure 4. Development of an instrument control using our established acquisition method (column #5, 90 min gradient, cond4 for DDA, and condB for DIA runs). (A) Experimental strategy for implementation of an instrument performance qualification for large-scale proteomic measurements of cell therapies. (B) Extracted ion chromatogram for the AVGANPEQLTR peptide (m/z 583.3136, z = 2+) and representative mass spectrum (inset). (C) Some metrics of control for nanoLC measurements using the PepCalMix, here showcasing the AVGANPEQLTR peptide. (D) Control metrics for the measurements of a complex commercial digest in DDA mode using protein and peptide identifications. (E) DIA control metrics. The selection of the proteins for DIA control is presented in Figure S7. The dots represent the mean quantitative values, and the whiskers span 3 × standard deviation. Key: blue lines indicate high and low limits for system compliance; red line indicates the median measurements; RT, retention time; Res., resolution; Int., intensity.

https://doi.org/10.1021/acs.jproteome.1c00887
J. Proteome Res. 2022, 21, 1229−1239

punctual mass calibration using a calibration LC run. The calibration LC run is specific to the TripleTOF 6600+ system used for this study; punctual calibration should be performed as needed following the mass spectrometer manufacturer recommendations. After the calibration run is completed, a calibration report containing data on peptide ions intensities, mass resolution for each peptide, retention times, and mass accuracy for MS1 and MS2 levels is produced. We present some representative data for one select peptide from the PepCalMix (Figure 4B,C). The K562 digest was run in both DDA mode (K562(D)) and SWATH acquisition mode (K562(S)). The K562 digest helps assessing the ion source, the MS1 and MS2 signals, dynamic ion sampling, and peptide identification (Figure 4D).

Using the PepCalMix AutoCal runs in our instrument, we can track the performances of the nanoLC-MS system over time. Key parameters to monitor are presented in Figure 4BC for the select peptide AVGANPEQLTR (m/z 583.3136, z = 2+). By monitoring the extracted ion chromatograms for each of the peptides contained in the PepCalMix, we can evaluate the efficiency of the separation (Figure 4B). For example, we show that the peak-width-at-half-maximum for the AVGANPEQLTR peptide was ≈0.05 min, representing ≈875 000 plate numbers. For most of the peptides, we recorded plate numbers between ≈175 000 and 675 000.

From the generated calibration reports, we extracted the information on the retention time (RT), the mass resolution (Res), and the intensity (Int) for each peptide across different days. On the basis of the collected data, we established thresholds that the system must meet to be considered compliant and for the analysis to move forward, beyond the ability of the mass spectrometer to perform the automated mass calibration in both MS and MS/MS modes. For RTs, the high and low thresholds were defined as 3 × standard deviation of the mean. We defined low-pass thresholds only for resolution and intensity, based on manufacturer recommendations and empirical data. We can evaluate more parameters using the complex digest (K562), including the data processing pipeline (Figure 4D). In DDA mode, we established a low pass number of proteins and peptides that we expect to be identified, based on a 3 × standard deviation of the mean. Here, we expect our protein identification to be higher than 3350 proteins and 26 900 peptides for 1 μg of digest on the column and a 90 min gradient (Figure 4D, top). We also completed the evaluation of the K562 digest in DIA mode (Figure 4D, bottom). Using the 18 K562 DIA runs performed to establish the LLODs and LLOQs, we created a list of 20 proteins spanning the entirety of the quantification range, presenting RSDs below 10% present in all 18 runs. The selection of the proteins based on their quantitative values is shown in Figure S7. These PQ samples control for our platform's quantitative repeatability and reproducibility without the variation existing in lab-prepared biological samples. In our measurement control design, we recommend performing two DIA runs at the beginning of the sample sequence and one at the end to assess any discrepancies potentially occurring between the first and last sample.

Overall, the instrument and data collection control presented here enables a robust and reproducible MS data collection for the measurements of scarce samples. The different thresholds presented in this manuscript are specific to our LC-MS instrument setup and represent a guideline more than hard-set values. Different instruments likely produce different results and require careful evaluation before starting any measurements of biopharma or clinically relevant samples. For example, in the sections above, we demonstrated that different columns led to different metrics in peak shape, retention times, number of proteins and peptides identifications, and quantitative metrics. Our control strategy design applies to DIA experiments on any instrument, but the thresholds should be evaluated on a case-by-case basis.

Application of Our DIA Approach to a Jurkat Cell Sample

To evaluate our method on a sample relevant to our application, we performed DIA on Jurkat cell samples (Figure 5). Jurkat cells are immortalized, cancer T-cells, which are similar to primary patient's T-cells and can serve as a model system for T-cell-based therapies. Indeed, our main target application is to study the proteomic changes linked to the manufacturing of CAR-T cells, which are directly derived from patient's T-cells. The proteins from the cells were extracted and digested using the S-TRAP protocol.[40] From ≈500 ng of proteins on the column, we were able to quantify a total of ≈2500 proteins spanning 4-orders of magnitude (Figure 5A). Among the quantified proteins, we found critical markers of T-cells. For example, we were able to quantify the four extracellular subunits of the T-cell receptor complex (CD3E,

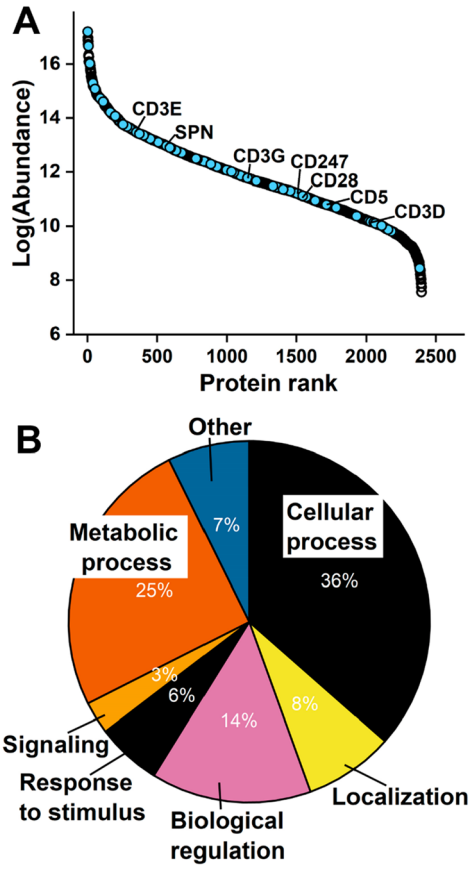

Figure 5. Application of our acquisition method to a T-cell model case—Jurkat cells. (A) Protein quantification by DIA of Jurkat cells prepared by S-TRAP lysis and digestion method. Proteins highlighted by sky-blue dots relate to T-cell biology. Some proteins, typically used as markers for T-cell identification, are identified in the graph. (B) Gene ontology annotation of biological processes occurring in unmodified Jurkat cells. The subclassification for the cellular and metabolic processes are presented in Figure S8.

https://doi.org/10.1021/acs.jproteome.1c00887
J. Proteome Res. 2022, 21, 1229−1239

CD3G, CD247, and CD3D),[41−43] the receptor CD5,[44] the receptor CD28,[45,46] and the transmembrane cell surface protein leukosialin (SPN or CD43).[47] Together, these markers are often used to isolate T-cells from plasma by fluorescence activated cell sorting. These CD receptors are required for T-cell activation and are present in all stages of T-cell differentiation.

Using gene ontology (GO) annotation, here using PantherDB,[48] we could map the quantified proteins to the leading cellular functions (Figure 5B). These data can now serve as a baseline to study the effect of engineering T-cells/Jurkat cells to express proteins of choice on their surfaces, such as a CAR. Moreover, after establishing a set sample preparation protocol, these types of data are helpful as metrics for a complete system suitability standard, which controls for the sample preparation and the instrument.

CONCLUSIONS

We have developed a sensitive DIA method to enable the measurements of emerging cell therapy products. We also established a PQ control strategy to ensure the method's reproducibility. Our control strategy was based on the MSQC principles, which evaluate key components of the LC-MS instrument and data acquisition. The method can potentially be applied in a regulated environment, as encountered in the biopharma industry using this stringent control strategy. Moreover, we applied the approach to Jurkat cells and were able to identify important markers of T-cells that can be used later as metrics to design complete system suitability standards.

ASSOCIATED CONTENT

Supporting Information

The Supporting Information is available free of charge at https://pubs.acs.org/doi/10.1021/acs.jproteome.1c00887.

Table S1, Columns and gradients description used for the commercial complex protein digest; Table S2, Description of the different gradient used to test the gradient length; Table S3 Description of the parameters that were modified to improve peptide detection in DDA mode; Table S4, Description of the parameters that were modified to improve peptide detection in DIA mode; Figure S1, Results for protein quantification by DIA of 200 ng of K562 digest; Figure S2, Chromatographic peak width and acquisition redundancy for peptides identified in DDA experiments with different gradient durations; Figure S3, Quantification technical reproducibility measured by RSD frequency for each gradient time and each DIA condition; Figure S4, Distribution of m/z for K562 digest and Jurkat cells digest; Figure S5, Comparison of the protein quantitative ranges with the different DIA acquisition methods for all proteins and the one unique to the two variable windows DIA methods; Figure S6, Representative quantitative calibration curve for the select peptide; Figure S7, Dynamic range observed for the K562 digest acquired in DIA mode and proteins selected for PQ monitoring; Figure S8, Subclassification of the metabolic process and cell process gene ontologies (PDF)

Table S5, Summary of supporting data from protein identification by DDA (XLSX)

Table S6, Summary of supporting data from protein quantification by SWATH-MS (XLSX)

AUTHOR INFORMATION

Corresponding Authors

Camille Lombard-Banek − *National Institute of Standards and Technology, Material and Measurements Laboratory, Gaithersburg, Maryland 20899, United States; Institute for Bioscience and Bioengineering Research, Rockville, Maryland 20850, United States;* orcid.org/0000-0003-0438-1042; Email: clombard@umd.edu

John E. Schiel − *National Institute of Standards and Technology, Material and Measurements Laboratory, Gaithersburg, Maryland 20899, United States; Institute for Bioscience and Bioengineering Research, Rockville, Maryland 20850, United States*; Email: john.schiel@nist.gov

Authors

Kerstin I. Pohl − *SCIEX, Framingham, Massachusetts 01701, United States*

Edward J. Kwee − *National Institute of Standards and Technology, Material and Measurements Laboratory, Gaithersburg, Maryland 20899, United States*

John T. Elliott − *National Institute of Standards and Technology, Material and Measurements Laboratory, Gaithersburg, Maryland 20899, United States*

Complete contact information is available at: https://pubs.acs.org/10.1021/acs.jproteome.1c00887

Author Contributions

C.L.-B. and J.E.S. designed the study. C.L.-B., J.E.S., and K.I.P. planned the experiments. E.J.K. and J.T.E. provided the Jurkat cell samples. C.L.-B. performed the experiments. C.L.-B. and J.E.S. wrote the manuscript. All the authors commented on the manuscript.

Notes

The authors declare no competing financial interest.

Raw Data: Raw data were deposited to the ProteomeXchange database (PXD029780). R Code: The R script used to interpret the data was deposited to GitHub (https://github.com/Lombardbanekc/CART-SWATH-MS-Data-Processing.git). "DDA Analysis_K562.R" was used to extract and filter the protein and peptide identifications from the ProteinPilot search results. "DDA summary.R" compiles the number of protein and peptide identifications after extracting the information using the "DDA Analysis_K562.R" script. "SWATH PepCal Quant.R" performs statistical analysis for the quantitative analysis of PepCal mix spiked in the K562 protein digest. "SWATH data processing.R" was used to process all other quantitative experiments using DIA.

Commercial equipment, instruments, or materials are identified in this paper to specify the experimental procedure adequately. Such identification is not intended to imply recommendation or endorsement by the National Institute of Standards and Technology, nor is it intended to imply that the materials or equipment identified are necessarily the best available for the purpose.

ACKNOWLEDGMENTS

We thank M. C. Burke and B. A. Neely for their helpful review of this manuscript. We also thank the National Research Council (NRC) for support through the NRC postdoctoral fellowship program (to C.L-B.).

https://doi.org/10.1021/acs.jproteome.1c00887
J. Proteome Res. 2022, 21, 1229−1239

REFERENCES

(1) Vormittag, P.; Gunn, R.; Ghorashian, S.; Veraitch, F. S. A guide to manufacturing CAR T cell therapies. *Curr. Opin. Biotechnol.* **2018**, *53*, 164−181.

(2) Wang, X.; Riviere, I. Clinical manufacturing of CAR T cells: foundation of a promising therapy. *Molecular therapy oncolytics* **2016**, *3*, 16015−16021.

(3) Meyer, C.; Rutjens, E.; Merlin, T. An introduction to analytics for autologous cell and gene therapies. *Chimia* **2020**, *74* (3), 193−193.

(4) Fischer, J. W.; Bhattarai, N. CAR-T cell therapy: mechanism, management, and mitigation of inflammatory toxicities. *Front. Immunol.* **2021**, *12*, 1−9.

(5) Pettitt, D.; Arshad, Z.; Smith, J.; Stanic, T.; Hollander, G.; Brindley, D. CAR-T cells: a systematic review and mixed methods analysis of the clinical trial landscape. *Molecular Therapy* **2018**, *26* (2), 342−353.

(6) Eyles, J. E.; Vessillier, S.; Jones, A.; Stacey, G.; Schneider, C. K.; Price, J. Cell therapy products: focus on issues with manufacturing and quality control of chimeric antigen receptor T-cell therapies. *J. Chem. Technol. Biotechnol.* **2019**, *94* (4), 1008−1016.

(7) Highfill, S. L.; Stroncek, D. F. Overcoming challenges in process development of cellular therapies. *Current Hematologic Malignancy Reports* **2019**, *14* (4), 269−277.

(8) Lombard-Banek, C.; Schiel, J. E. Mass spectrometry advances and perspectives for the characterization of emerging adoptive cell therapies. *Molecules* **2020**, *25* (6), 1−26.

(9) Neilson, K. A.; Ali, N. A.; Muralidharan, S.; Mirzaei, M.; Mariani, M.; Assadourian, G.; Lee, A.; van Sluyter, S. C.; Haynes, P. A. Less label, more free: Approaches in label-free quantitative mass spectrometry. *Proteomics* **2011**, *11* (4), 535−553.

(10) Zhang, Y. Y.; Fonslow, B. R.; Shan, B.; Baek, M. C.; Yates, J. R. Protein analysis by shotgun/bottom-up proteomics. *Chem. Rev.* **2013**, *113* (4), 2343−2394.

(11) Pappireddi, N.; Martin, L.; Wuhr, M. A review on quantitative multiplexed proteomics. *Chembiochem* **2019**, *20* (10), 1210−1224.

(12) McAlister, G. C.; Huttlin, E. L.; Haas, W.; Ting, L.; Jedrychowski, M. P.; Rogers, J. C.; Kuhn, K.; Pike, I.; Grothe, R. A.; Blethrow, J. D.; Gygi, S. P. Increasing the multiplexing capacity of TMTs using reporter ion isotopologues with isobaric masses. *Anal. Chem.* **2012**, *84* (17), 7469−7478.

(13) Geiger, T.; Cox, J.; Mann, M. Proteomics on an orbitrap benchtop mass spectrometer using all-ion fragmentation. *Molecular & Cellular Proteomics* **2010**, *9* (10), 2252−2261.

(14) Collins, B. C.; Gillet, L. C.; Rosenberger, G.; Rost, H. L.; Vichalkovski, A.; Gstaiger, M.; Aebersold, R. Quantifying protein interaction dynamics by SWATH mass spectrometry: application to the 14−3-3 system. *Nat. Methods* **2013**, *10* (12), 1246−1253.

(15) Rogers, R. S.; Nightlinger, N. S.; Livingston, B.; Campbell, P.; Bailey, R.; Balland, A. Development of a quantitative mass spectrometry multi-attribute method for characterization, quality control testing and disposition of biologics. *Mabs* **2015**, *7* (5), 881−890.

(16) Mouchahoir, T.; Schiel, J. E.; Rogers, R.; Heckert, A.; Place, B. J.; Ammerman, A.; Li, X. X.; Robinson, T.; Schmidt, B.; Chumsae, C. M.; Li, X. B.; Manuilov, A. V.; Yan, B.; Staples, G. O.; Ren, D.; Veach, A. J.; Wang, D. D.; Yared, W.; Sosic, Z.; Wang, Y.; Zang, L.; Leone, A. M.; Liu, P. R.; Ludwig, R.; Tao, L.; Wu, W.; Cansizoglu, A.; Hanneman, A.; Adams, G. W.; Perdivara, I.; Walker, H.; Wilson, M.; Brandenburg, A.; DeGraan-Weber, N.; Gotta, S.; Shambaugh, J.; Alvarez, M.; Yu, X. C.; Cao, L.; Shao, C.; Mahan, A.; Nanda, H.; Nields, K.; Nightlinger, N.; Barysz, H. M.; Jahn, M.; Niu, B.; Wang, J. H.; Leo, G.; Sepe, N.; Liu, Y. H.; Patel, B. A.; Richardson, D.; Wang, Y.; Tizabi, D.; Borisov, O. V.; Lu, Y. L.; Maynard, E. L.; Gruhler, A.; Haselmann, K. F.; Krogh, T. N.; Sonksen, C. P.; Letarte, S.; Shen, S.; Boggio, K.; Johnson, K.; Ni, W. Q.; Patel, H.; Ripley, D.; Rouse, J. C.; Zhang, Y.; Daniels, C.; Dawdy, A.; Friese, O.; Powers, T. W.; Sperry, J. B.; Woods, J.; Carlson, E.; Sen, K. I.; Skilton, S.; Busch, M.; Lund, A.; Stapels, M.; Guo, X.; Heidelberger, S.; Kaluarachchi, H.; McCarthy, S.; Kim, J.; Zhen, J.; Zhou, Y.; Rogstad, S.; Wang, X. S.; Fang, J.; Chen, W. B.; Yu, Y. Q.; Hoogerheide, J. G.; Scott, R.; Yuan, H. New peak detection performance metrics from the MAM consortium interlaboratory study. *J. Am. Soc. Mass Spectrom.* **2021**, *32* (4), 913−928.

(17) Li, K. W.; Gonzalez-Lozano, M. A.; Koopmans, F.; Smit, A. B. Recent developments in data independent acquisition (DIA) mass spectrometry: application of quantitative analysis of the brain proteome. *Front. Mol. Neurosci.* **2020**, *13*, 1−8.

(18) Gillet, L. C.; Navarro, P.; Tate, S.; Rost, H.; Selevsek, N.; Reiter, L.; Bonner, R.; Aebersold, R. Targeted data extraction of the MS/MS spectra generated by data-independent acquisition: A new concept for consistent and accurate proteome analysis. *Mol. Cell. Proteomics* **2012**, *11* (6), O111.016717.

(19) Piening, B. D.; Wang, P.; Bangur, C. S.; Whiteaker, J.; Zhang, H. D.; Feng, L. C.; Keane, J. F.; Eng, J. K.; Tang, H.; Prakash, A.; McIntosh, M. W.; Paulovich, A. Quality control metrics for LC-MS feature detection tools demonstrated on Saccharomyces cerevisiae proteomic profiles. *J. Proteome Res.* **2006**, *5* (7), 1527−1534.

(20) Rudnick, P. A.; Clauser, K. R.; Kilpatrick, L. E.; Tchekhovskoi, D. V.; Neta, P.; Blonder, N.; Billheimer, D. D.; Blackman, R. K.; Bunk, D. M.; Cardasis, H. L.; Ham, A. J. L.; Jaffe, J. D.; Kinsinger, C. R.; Mesri, M.; Neubert, T. A.; Schilling, B.; Tabb, D. L.; Tegeler, T. J.; Vega-Montoto, L.; Variyath, A. M.; Wang, M.; Wang, P.; Whiteaker, J. R.; Zimmerman, L. J.; Carr, S. A.; Fisher, S. J.; Gibson, B. W.; Paulovich, A. G.; Regnier, F. E.; Rodriguez, H.; Spiegelman, C.; Tempst, P.; Liebler, D. C.; Stein, S. E. Performance metrics for liquid chromatography-tandem mass spectrometry systems in proteomics analyses. *Molecular & Cellular Proteomics* **2010**, *9* (2), 225−241.

(21) Bittremieux, W.; Tabb, D. L.; Impens, F.; Staes, A.; Timmerman, E.; Martens, L.; Laukens, K. Quality control in mass spectrometry-based proteomics. *Mass Spectrom. Rev.* **2018**, *37* (5), 697−711.

(22) Dogu, E.; Mohammad-Taheri, S.; Abbatiello, S. E.; Bereman, M. S.; MacLean, B.; Schilling, B.; Vitek, O. MSstatsQC: longitudinal system suitability monitoring and quality control for targeted proteomic experiments. *Molecular & Cellular Proteomics* **2017**, *16* (7), 1335−1347.

(23) Bittremieux, W.; Walzer, M.; Tenzer, S.; Zhu, W. M.; Salek, R. M.; Eisenacher, M.; Tabb, D. L. The Human proteome organization-proteomics standards initiative quality control working group: making quality control more accessible for biological mass spectrometry. *Anal. Chem.* **2017**, *89* (8), 4474−4479.

(24) Morgenstern, D.; Barzilay, R.; Levin, Y. RawBeans: a simple, vendor-independent, raw-Data quality-control tool. *J. Proteome Res.* **2021**, *20* (4), 2098−2104.

(25) Salter, A. I.; Ivey, R. G.; Kennedy, J. J.; Voillet, V.; Rajan, A.; Alderman, E. J.; Voytovich, U. J.; Lin, C. W.; Sommermeyer, D.; Liu, L. F.; Whiteaker, J. R.; Gottardo, R.; Paulovich, A. G.; Riddell, S. R. Phosphoproteomic analysis of chimeric antigen receptor signaling reveals kinetic and quantitative differences that affect cell function. *Sci. Signal.* **2018**, *11* (544), No. eaat6753.

(26) Ramello, M. C.; Benzaid, I.; Kuenzi, B. M.; Lienlaf-Moreno, M.; Kandell, W. M.; Santiago, D. N.; Pabon-Saldana, M.; Darville, L.; Fang, B.; Rix, U.; Yoder, S.; Berglund, A.; Koomen, J. M.; Haura, E. B.; Abate-Daga, D. An immunoproteomic approach to characterize the CAR interactome and signalosome. *Sci. Signal.* **2019**, *12* (568), No. eaap9777.

(27) Griffith, A. A.; Callahan, K. P.; King, N. G.; Xiao, Q.; Su, X.; Salomon, A. R. SILAC phosphoproteomics reveals unique signaling circuits in CAR-T cells and the inhibition of B cell-activating phosphorylation in target cells. *J. Proteome Res.* **2022**, *21* (2), 395−409.

(28) Bloemberg, D.; Nguyen, T.; MacLean, S.; Zafer, A.; Gadoury, C.; Gurnani, K.; Chattopadhyay, A.; Ash, J.; Lippens, J.; Harcus, D.; Page, M.; Fortin, A.; Pon, R. A.; Gilbert, R.; Marcil, A.; Weeratna, R. D.; McComb, S. A high-throughput method for characterizing novel chimeric antigen receptors in Jurkat cells. *Molecular Therapy-Methods & Clinical Development* **2020**, *16*, 238−254.

https://doi.org/10.1021/acs.jproteome.1c00887
J. Proteome Res. 2022, 21, 1229−1239

(29) Seymour, S. L.; Shilov, I. V.; Patel, A. A.; Loboda, A.; Tang, W. H.; Keating, S. P.; Schaeffer, D. A. The paragon algorithm: A sequence tagbased search engine that substantially improves peptide identification by using sequence temperatures and feature probabilities. *Mol. Cell. Proteomics* **2006**, *5* (10), S293−S293.
(30) Shilov, I. V.; Seymour, S. L.; Patel, A. A.; Loboda, A.; Tang, W. H.; Keating, S. P.; Hunter, C. L.; Nuwaysir, L. M.; Schaeffer, D. A. The paragon algorithm, a next generation search engine that uses sequence temperature values and feature probabilities to identify peptides from tandem mass spectra. *Molecular & Cellular Proteomics* **2007**, *6* (9), 1638−1655.
(31) Gilar, M.; Daly, A. E.; Kele, M.; Neue, U. D.; Gebler, J. C. Implications of column peak capacity on the separation of complex peptide mixtures in single- and two-dimensional high-performance liquid chromatography. *Journal of Chromatography, A* **2004**, *1061* (2), 183−192.
(32) Lombard-Banek, C.; Moody, S. A.; Nemes, P. Single-cell mass spectrometry for discovery proteomics: quantifying translational cell heterogeneity in the 16-cell frog (*Xenopus*) embryo. *Angew. Chem., Int. Ed.* **2016**, *55* (7), 2454−2458.
(33) Lombard-Banek, C.; Yu, Z.; Swiercz, A. P.; Marvar, P. J.; Nemes, P. A microanalytical capillary electrophoresis mass spectrometry assay for quantifying angiotensin peptides in the brain. *Anal. Bioanal. Chem.* **2019**, *411* (19), 4661−4671.
(34) Zhu, Y.; Zhao, R.; Piehowski, P. D.; Moore, R. J.; Lim, S.; Orphan, V. J.; Pasa-Tolic, L.; Qian, W. J.; Smith, R. D.; Kelly, R. T. Subnanogram proteomics: Impact of LC column selection, MS instrumentation and data analysis strategy on proteome coverage for trace samples. *Int. J. Mass Spectrom.* **2018**, *427*, 4−10.
(35) Bruderer, R.; Bernhardt, O. M.; Gandhi, T.; Xuan, Y.; Sondermann, J.; Schmidt, M.; Gomez-Varela, D.; Reiter, L. Optimization of experimental parameters in data-independent mass spectrometry significantly increases depth and reproducibility of results. *Molecular & Cellular Proteomics* **2017**, *16* (12), 2296−2309.
(36) Li, S. S.; Cao, Q. C.; Xiao, W. D.; Guo, Y. F.; Yang, Y. F.; Duan, X. X.; Shui, W. Q. Optimization of acquisition and data-processing parameters for improved proteomic quantification by sequential window acquisition of all theoretical fragment ion mass spectrometry. *J. Proteome Res.* **2017**, *16* (2), 738−747.
(37) Doellinger, J.; Blumenscheit, C.; Schneider, A.; Lasch, P. Isolation window optimization of data-independent acquisition using predicted libraries for deep and accurate proteome profiling. *Anal. Chem.* **2020**, *92* (18), 12185−12192.
(38) Pino, L. K.; Just, S. C.; MacCoss, M. J.; Searle, B. C. Acquiring and analyzing data independent acquisition proteomics experiments without spectrum libraries. *Molecular & Cellular Proteomics* **2020**, *19* (7), 1088−1103.
(39) Messner, C. B.; Demichev, V.; Bloomfield, N.; Yu, J. S. L.; White, M.; Kreidl, M.; Egger, A. S.; Freiwald, A.; Ivosev, G.; Wasim, F.; Zelezniak, A.; Jurgens, L.; Suttorp, N.; Sander, L. E.; Kurth, F.; Lilley, K. S.; Mulleder, M.; Tate, S.; Ralser, M. Ultra-fast proteomics with Scanning SWATH. *Nat. Biotechnol.* **2021**, *39* (7), 846−854.
(40) Elinger, D.; Gabashvili, A.; Levin, Y. Suspension trapping (S-Trap) is compatible with typical protein extraction buffers and detergents for bottom-up proteomics. *J. Proteome Res.* **2019**, *18* (3), 1441−1445.
(41) Lever, M.; Maini, P. K.; van der Merwe, P. A.; Dushek, O. Phenotypic models of T cell activation. *Nature Reviews Immunology* **2014**, *14* (9), 619−629.
(42) Courtney, A. H.; Lo, W. L.; Weiss, A. TCR Signaling: Mechanisms of Initiation and Propagation. *Trends Biochem. Sci.* **2018**, *43* (2), 108−123.
(43) Liu, B. Y.; Kolawole, E. M.; Evavold, B. D. Mechanobiology of T Cell Activation: To Catch a Bond. *Annu. Rev. Cell Dev. Biol.* **2021**, *37*, 65−87.
(44) Voisinne, G.; de Peredo, A. G.; Roncagalli, R. CD5, an Undercover Regulator of TCR Signaling. *Front. Immunol.* **2018**, DOI: 10.3389/fimmu.2018.02900.
(45) Esensten, J. H.; Helou, Y. A.; Chopra, G.; Weiss, A.; Bluestone, J. A. CD28 Costimulation: From Mechanism to Therapy. *Immunity* **2016**, *44* (5), 973−988.
(46) Rudd, C. E.; Taylor, A.; Schneider, H. CD28 and CTLA-4 coreceptor expression and signal transduction. *Immunological Reviews* **2009**, *229*, 12−26.
(47) Zadeh, A. D.; Seveau, S.; Halbwachs-Mecarelli, L.; Keller, H. U. Chemotactically-induced redistribution of CD43 as related to polarity and locomotion of human polymorphonuclear leucocytes. *Biology of the Cell* **2003**, *95* (5), 265−273.
(48) Mi, H. Y.; Ebert, D.; Muruganujan, A.; Mills, C.; Albou, L. P.; Mushayamaha, T.; Thomas, P. D. PANTHER version 16: a revised family classification, tree-based classification tool, enhancer regions and extensive API. *Nucleic Acids Res.* **2021**, *49* (D1), D394−D403.

https://doi.org/10.1021/acs.jproteome.1c00887
J. Proteome Res. 2022, 21, 1229−1239